Computer simulations of the ordering in a hybrid cylindrical film of nematic liquid crystals

C. Chiccoli,[1] P. Pasini,[1] R. Teixeira de Souza,[2] L. R. Evangelista,[2] and C. Zannoni[3]
[1]*Istituto Nazionale di Fisica Nucleare, Sezione di Bologna, Via Irnerio 46, I-40126 Bologna, Italy*
[2]*Departamento de Física, Universidade Estadual de Maringá Avenida Colombo, 5790-87020-900 Maringá-PR, Brazil*
[3]*Dipartimento di Chimica Fisica and INSTM, Università, Viale Risorgimento 4, I-40136 Bologna, Italy*
(Received 30 May 2011; published 21 October 2011)

We present an investigation of the ordering in a nematic liquid-crystal film confined between two cylindrical surfaces with antagonistic (radial and planar) anchoring alignments. A Monte Carlo study of a Lebwohl-Lasher model with suitable boundary conditions has been performed to calculate the ordering and the molecular organization for different film thicknesses. The simulation results are compared with some theoretical predictions obtained with the elastic continuum approach. The agreement between theory and simulation is improved as the thickness decreases.

DOI: 10.1103/PhysRevE.84.041705 PACS number(s): 61.30.Cz, 61.30.Hn, 61.30.Gd, 61.30.Pq

I. INTRODUCTION

The study of confined nematic systems has attracted and is attracting a great deal of interest both from the theoretical and experimental point of view [1]. In the last few years we have employed Monte Carlo computer simulations to investigate at a microscopic level some of these systems [2]. In particular, we have studied different geometries, such as droplets, cylinders, and films for various boundary conditions, anchoring strengths, external fields, etc. We have shown that this computational approach is very useful not only in determining the thermodynamic observables of the system but also the molecular organization that results from the competition of the above mentioned conditions. On the other hand, the continuum elastic theory has been a useful tool for investigating some phenomena in nonplanar geometry, in which unusual consequences have been found [3–10]. Here we have started to combine the simulation and continuum theory approaches to investigate the problem of nematics confined between concentric cylindrical surfaces [11,12]. Even though the model, described in the next section, is very simple, we have shown that it is sufficient to describe adequately systems where experimental results are available, as it proved possible for spherical Polymer Dispersed Liquid Crystals (PDLC) droplets [13–15] and thin films [16–18]. The model has also been used to study a nematic confined into a cylindrical pore [19,20] for which experimental studies exist [21]. The aim of the present work is to study the effect on molecular organization of antagonist boundaries on the two cylindrical surfaces and of exchanging the inside and outside anchoring conditions. We confirm, as possibly expected, that the distortions can be strongly different even for a simple switch of the boundary conditions, and that they tend to be more similar as the cylindrical film thickness decreases. After a brief description of the simulation model, we present some Monte Carlo results obtained for some thickness values. Then a simple elastic model is developed and used to compare the analytical predictions with the simulation results.

II. SIMULATION MODEL

The cylindrical film model sample $\mathcal{S}$ used in simulations is obtained carving two concentric cylinders from a cubic lattice with spins at lattice points interacting with the Lebwohl-Lasher (LL) potential [22] [Eq. (1)]. The cylindrical shell obtained has outer and inner diameters r_2 and r_1, respectively, and a height of m lattice layers. This model is well known for reproducing the main orientational features of nematic liquid crystals. The surface effects of the inner and outer surfaces are modeled with two external layers of "ghost" spins, $\mathcal{G}_{\rm in}$ and $\mathcal{G}_{\rm out}$, with fixed orientations chosen to mimic the desired boundary conditions. The boundary layers act on the inside particles according to the simple pair interaction:

$$U_{i,j} = -\epsilon_{ij} J\left[\frac{3}{2}(\mathbf{u}_i \cdot \mathbf{u}_j)^2 - \frac{1}{2}\right], \quad \text{for} \quad i \in \mathcal{S},\ j \in \mathcal{G}_{\rm in} \text{ or } j \in \mathcal{G}_{\rm out}, \tag{1}$$

where $\epsilon_{ij} = \epsilon$, with $\epsilon > 0$ for nearest neighbors i and j, and 0 otherwise; $\mathbf{u}_i$ and $\mathbf{u}_j$ are the orientations of the spins at sites i and j, respectively; and J denotes the relative strength of the coupling between a "nematic" and a surface spin compared to that between two nematic spins. Thus, when $J = 1$ the interaction between two neighbors, one on the surface of the nematic film and one belonging to the outside matrix, is the same as that between two liquid-crystal spins, while at the other extreme $J = 0$ would correspond to a film in a vacuum. Here we assume for simplicity $J = 1$.

In the present paper we have considered the following two different boundary conditions at the interfaces (see Fig. 1):

(*i*) *R-Z-BC*. This type has radial boundary conditions (homeotropic, RBC) at the outer surface, that are imposed by orienting the spins in the outside aligning layer normally to the local surface and pointing towards the center of the cylinder while the vertical orientation at the inner surface is implemented with spins all aligned along Z (ZBC).

(*ii*) *Z-R-BC*. The alignments at the surfaces are inverted with respect the previous case, i.e., ZBC at the outer surface and RBC at the inner surface.

For each of these cases we have performed a simulation deep in the nematic phase at a reduced temperature $T^* = 0.2$, where $T^* = kT/\varepsilon$ and k is the Boltzmann constant. We recall that in the bulk the nematic-isotropic phase transition occurs at a temperature $T^* = 1.1232$ [23] and that at $T^* = 0.2$ the orientational order $\langle P_2 \rangle_\lambda$, obtained from diagonalization of the ordering matrix [2], is $\approx$0.99. To examine the ordering inside the cylindrical film, various second rank order parameters have been calculated for the systems investigated. We

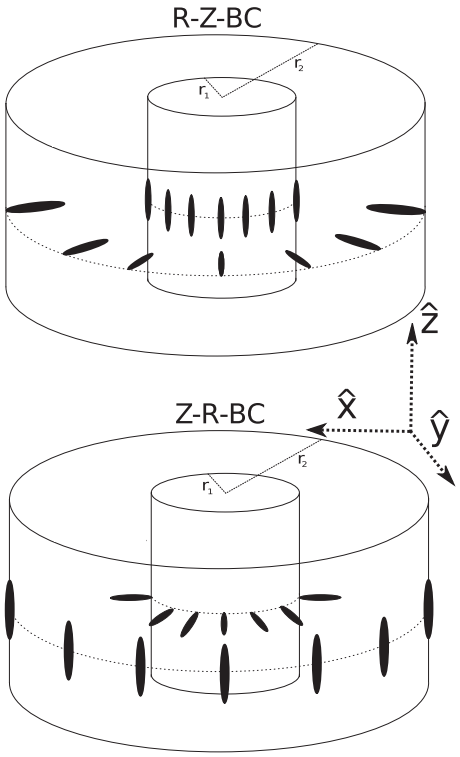

FIG. 1. Schematic representation of the cylindrical film geometry with the two boundary conditions studied.

notice that the ordinary second rank order parameter $\langle P_2\rangle_\lambda$ is not always appropriate as it quantifies the nematic order with respect to an hypothetical global director which may not exist as such in the present nonspatially uniform geometry. However, Monte Carlo (MC) simulations offer the possibility of evaluating some other order parameters more appropriate to each special case. For example, it is more useful to define a configurational order parameter, $\langle P_2\rangle_C$, which tends to one for a configuration perfectly ordered according to the idealized structure induced by the boundary conditions used (Fig. 1). Thus

$$\langle P_2\rangle_C = \frac{1}{N}\sum_{i=1}^{N} P_2(\mathbf{u}_i \cdot \mathbf{c}_i), \tag{2}$$

where $\mathbf{c}_i$ is a unit vector representing the ideal orientation at site i and N is the number of particles.

For example in the case of alignment along Z, we can consider the order parameter $\langle P_2\rangle_Z$ with $\mathbf{c}_i = \mathbf{z}$ which corresponds to a perfect order when all the molecules are oriented along the axis of the cylinder, i.e., $\mathbf{z}$. Alternatively, if we want to observe the deviation from a perfect radial organization, we can consider a radial order parameter $\langle P_2\rangle_r$ which is one where all the spins are oriented along the local radius $\mathbf{r}_i$, i.e., $\mathbf{c}_i = \mathbf{r}_i$, and would vanish when we have a perfectly aligned or completely random system.

III. SIMULATION

We have simulated various film thicknesses keeping the outer cylinder radius $r_2 = 21$ constant and varying the inner radius r_1 from 1 to 18; the details of the systems used are reported in Table I. The height of the sample was 8 nematic layers, and periodic boundary conditions were employed in this vertical direction. We have then investigated the behavior of the various order parameters across the sample with the aim of assessing the molecular organization inside the cylinder film. The starting configurations of the systems were chosen to be completely aligned along the Z direction, and the updating of the spin orientations proceeded according to the classic Metropolis Monte Carlo procedure [24]. In MC simulations the calculation of the order parameters across the sample can be performed by dividing the sample in concentric cylindrical shells and calculating the relevant quantities in each region

TABLE I. Data of the simulated cylindrical films. r_1 is the inner radius; N_{LC}, N_{S1}, and N_{S2} are the number of nematic particles, and the number of spins belonging to surfaces S_1 and S_2 respectively.

r_1	1	2	4	6	8	10	12	14	16	18
N_{LC}	10208	10144	9824	9344	8576	7712	6656	5312	3744	2080
N_{S1}	32	64	160	224	352	384	544	736	800	800
N_{S2}	928	928	928	928	928	928	928	928	928	928

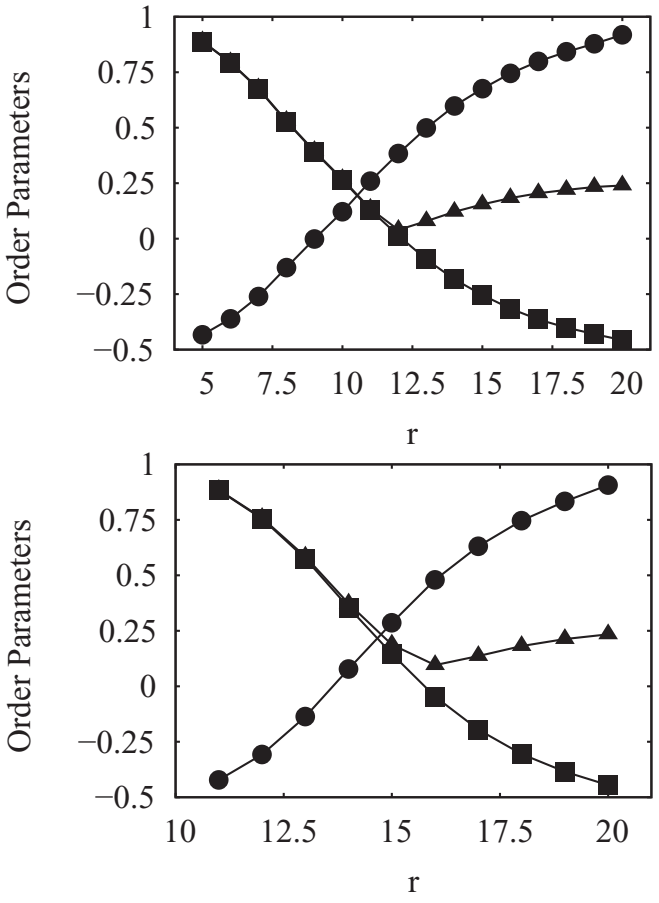

FIG. 2. Order parameters $\langle P_2\rangle_\lambda$ (triangles), $\langle P_2\rangle_r$ (circles), and $\langle P_2\rangle_Z$ (squares) in the R-Z-BC case starting from the inner surface. The results are for two different radii of the inner cylinder, i.e., $r_1 = 5$ (top) and and $r_1 = 11$ (bottom), while the radius of the outer cylinder is $r_2 = 21$. The values of $\langle P_2\rangle_\lambda$ (triangles) and $\langle P_2\rangle_Z$ (squares) are perfectly superimposed for low r

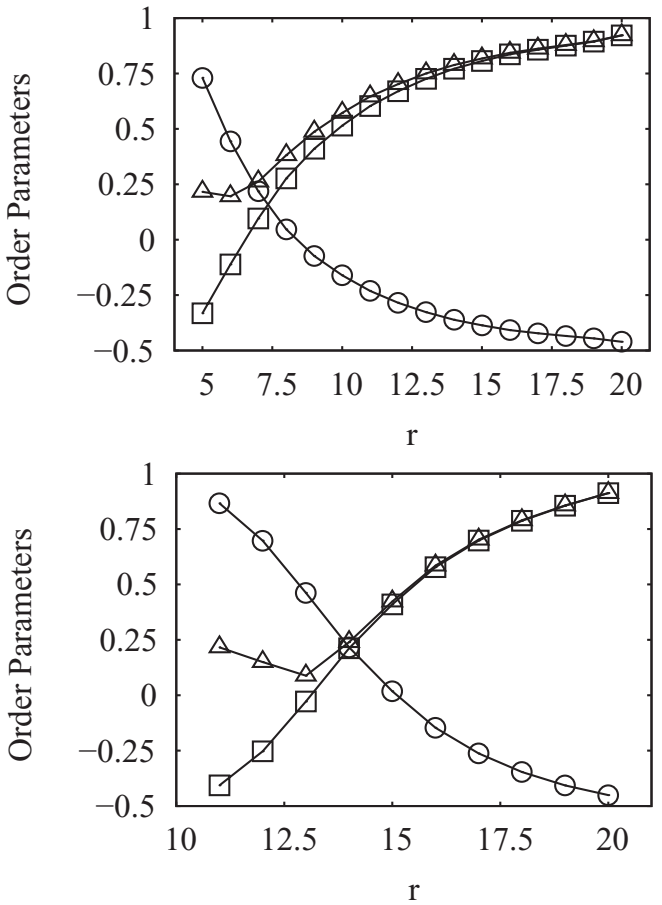

FIG. 3. Order parameters $\langle P_2\rangle_\lambda$ (triangles), $\langle P_2\rangle_r$ (circles), and $\langle P_2\rangle_Z$ (squares) in the Z-R-BC case starting from the inner surface. The results are for two different radii of the inner cylinder, i.e., $r_1 = 5$ (top) and and $r_1 = 11$ (bottom), while the radius of the outer cylinder is $r_2 = 21$.

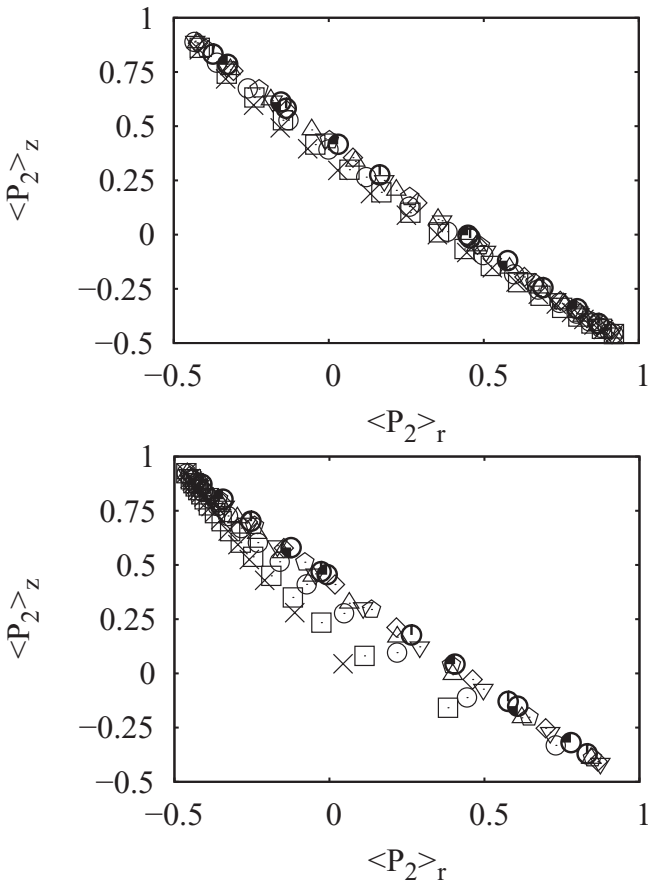

FIG. 4. Order parameters $\langle P_2\rangle_Z$ vs $\langle P_2\rangle_r$ for the R-Z-BC case (top) and Z-R-BC case (bottom) for the various values of r_1 (symbols as in Figs. 7 and 8). The deviation from the straight line in the Z-R-BC case for the thicker film is clear for data corresponding to the following inner radii: $r_1 = 1$ (crosses), $r_1 = 2$ (squares), and $r_1 = 3$ (circles).

so as to have the variation of the ordering on going from the center to the border of the system. As an example, the behavior of $\langle P_2\rangle_\lambda$, $\langle P_2\rangle_r$, and $\langle P_2\rangle_Z$ with respect to the distance from the inner to the outer surface for two different radii of the inner cylinder are reported in Fig. 2 for the R-Z-BC and in Fig. 3 for the Z-R-BC cases. It is clear from the plots in Fig. 2 that the radial order parameter has an opposite behavior in comparison with the $\langle P_2\rangle_Z$ which is maximum at the inner surface and about -0.5 at the outer boundary where the molecules are orthogonally oriented with respect to the Z direction. The standard nematic order parameter calculated with respect to the preferred direction of the layer starts from one close to the inner surface and after decreasing to a minimum close to the center of the film increases up to an average value which is the limit for a two dimensional (2D) random system. The different thicknesses of the cylindrical film do not seem to affect the behavior of the three order parameters.

Inverting the alignments at the cylindrical surfaces, the ordering inside the sample becomes very different when the thickness of the film increases. For larger thicknesses, keeping constant $r_2 = 21$ and decreasing r_1, we can observe that the influence of the aligning feature of the LL potential and the ordering along Z induced by the outer surface overcome the effect of the smaller number of radial particles located at the inner surface. This might be seen in Fig. 4 where $\langle P_2\rangle_Z$ is plotted against $\langle P_2\rangle_r$ for the various values of r_1 in the two cases R-Z-BC and Z-R-BC. In the first case [Fig. 4(a)] all the data points lie on a straight line $\langle P_2\rangle_Z = -\langle P_2\rangle_r + 1/2$, while for the Z-R-BC case [Fig. 4(b)] there are strong deviations from this line for the smaller inner radius r_1 corresponding to a larger film thickness. We can say that when the cylindrical film thickness is sufficiently small, the behavior is similar to that of a planar film for which there are no differences in exchanging the alignment at the surfaces. This is true also for the R-Z-BC case for all the thickness because the alignment along Z of a few molecules at the inner surface is sufficient, together with the aligning properties of the potential, to induce the ordering along Z of the sample up to the middle layers. On the contrary, a small number of molecules radially oriented at the inner surface (Z-R-BC case) does not influence the sample. These observations are more apparent by plotting together the two order parameters for the two cases for the different film thicknesses (Fig. 5).

To have an immediate qualitative view of the ordering of the system, we have plotted representative snapshots of the samples where each spin is given a color coding according to

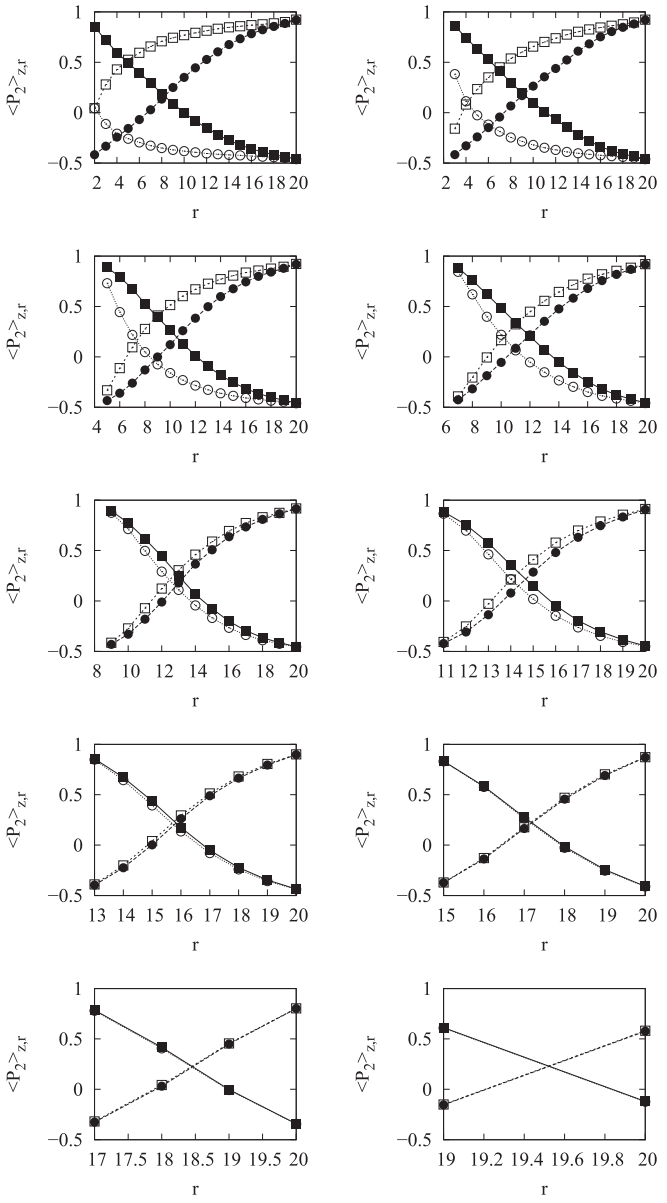

FIG. 5. Order parameters $\langle P_2\rangle_Z$ and $\langle P_2\rangle_r$ for the the Z-R-BC (empty symbols) and the R-Z-BC (full symbols) cases for the different film thicknesses with $r_1 = 1,2,4,6,8,10,12,14,16,18$.

its values of the alignment along the Z direction (cyano). The snapshots for some selected inner radius and for the two cases examined are presented in Figs. 6(a) and 6(b).

IV. ELASTIC THEORY

The deformations found with the Monte Carlo simulations can be analyzed in the Frank elastic theory context [25,26]. Because of the boundary conditions used in the simulations, the nematic director can be written just as $\vec{n} = \sin\phi\hat{r} + \cos\phi\hat{z}$, with ϕ the angle between $\vec{n}$ and $\hat{z}$. Since the cylinder is supposed to be homogeneous in θ and z, it is possible to assume that ϕ changes only with respect to the radial variable. As the simulations were performed with fixed molecules on the cylinder surface, this allows us to assume strong

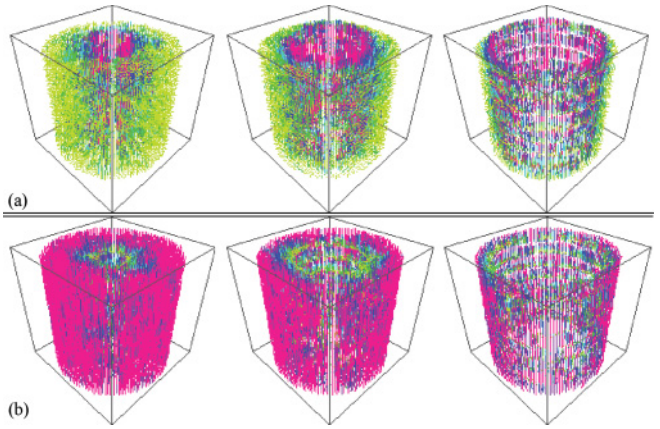

FIG. 6. (Color) Snapshots obtained by Monte Carlo simulations for the (a) R-Z-BC case and (b) Z-R-BC case for different radii of the inner cylinder, i.e., $r_1 = 4,10,16$ (from left to right).

anchoring with $\phi(r_1) = \Phi_1$ and $\phi(r_2) = \Phi_2$, for $\Phi_{1,2} = \pi/2$ and $\Phi_{2,1} = 0$ according to the situation considered.

From the elastic point of view, the Lebwohl-Lasher potential corresponds to one elastic constant approximation

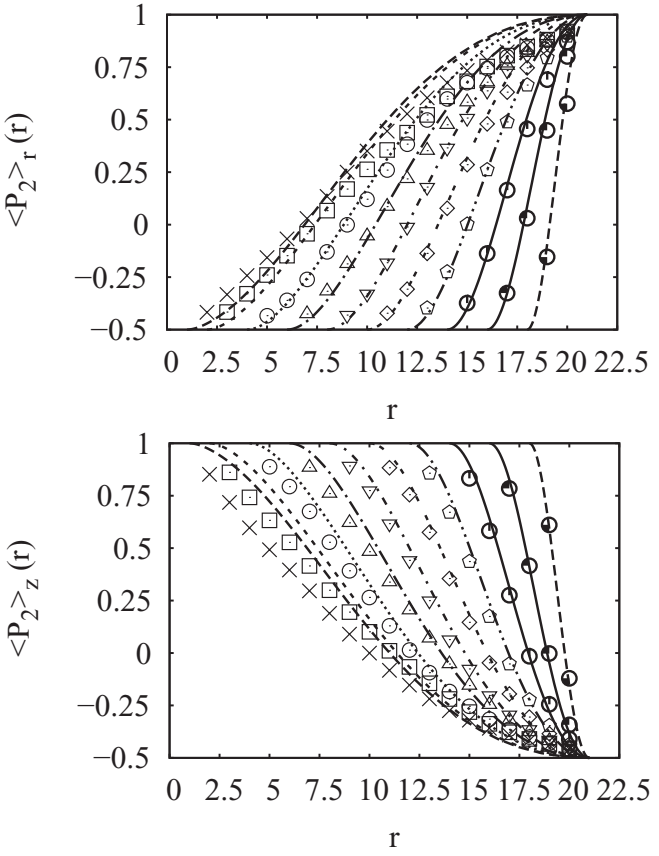

FIG. 7. Order parameters $\langle P_2\rangle_r$ and $\langle P_2\rangle_Z$ vs distance starting from the inner surface for the R-Z-BC case. The various curves refer to the different radii of the inner cylinder, i.e., $r_1 = 1,2,4,6,8,10,12,14,16,18$. The radius of the outer cylinder is $r_2 = 21$. The continuous lines are the elastic theory predictions while the points are the MC results.

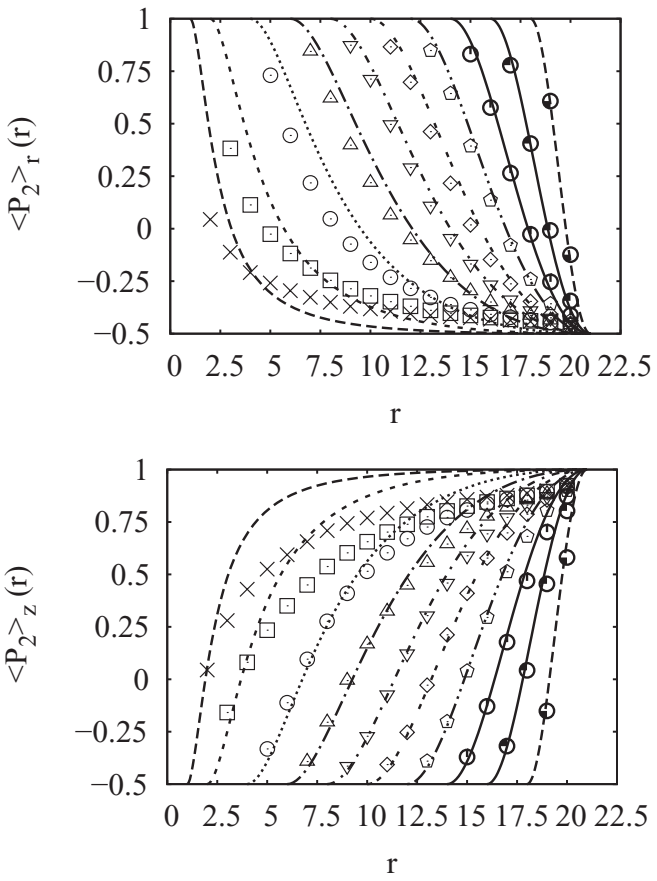

FIG. 8. Order parameters $\langle P_2\rangle_r$ and $\langle P_2\rangle_Z$ vs the distance starting from the inner surface for the Z-R-BC case. The various curves refer to the different radii of the inner cylinder, i.e., $r_1 = 1,2,4,6,8,10,12,14,16,18$. The radius of the outer cylinder is $r_2 = 21$. The continuous lines are the elastic theory predictions while the points are the MC results.

($K_{11} = K_{22} = K_{33} = K$), and the free energy density is given as

$$f_{EL} = \frac{K}{2}[(\vec{\nabla}\cdot\vec{n})^2 + (\vec{\nabla}\times\vec{n})^2]. \tag{3}$$

For the geometry we are considering here, the free energy per unit area can be written as

$$F = \pi K \int_{r_1}^{r_2} \left(\frac{\sin^2\phi(r)}{r^2} + \left[\frac{d\phi}{dr}\right]^2\right) r\,dr, \tag{4}$$

and has to be minimized according to the variational principle, thus leading us to search for the solutions of the nonlinear differential equation

$$\frac{d^2\phi}{dr^2} + \frac{1}{r}\frac{d\phi}{dr} - \frac{\sin 2\phi}{2r^2} = 0. \tag{5}$$

By integrating Eq. (5) it yields

$$\int_{\phi(r_1)}^{\phi(r)} \frac{d\xi}{\sqrt{\zeta - \cos^2\xi}} = \ln\left[\frac{r}{r_1}\right], \tag{6}$$

where ζ is an integration constant to be determined by imposing the boundary conditions. Thus, the solution $\phi(r)$ can be numerically obtained from Eq. (6).

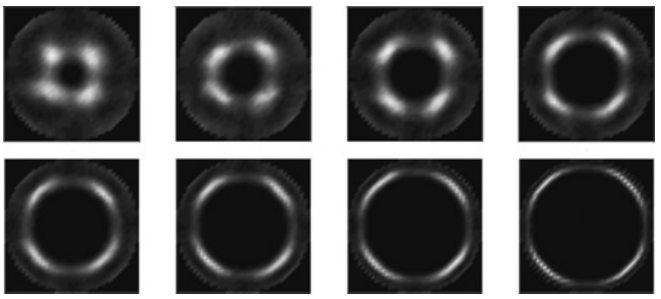

FIG. 9. Optical images (top view) as obtained by Monte Carlo simulations for the R-Z-BC case and different radii of the inner cylinder, i.e., $r_1 = 2,4,6,8,10,12,14,16$ (from top left to bottom right).

In order to compare the simulation data with the predictions of the elastic theory, we define the order parameter with respect to the radial direction as

$$\langle P_2\rangle_r^E(r) = \tfrac{3}{2}\cos^2\phi(r) - \tfrac{1}{2}, \tag{7}$$

and the order parameter with respect to z in the form

$$\langle P_2\rangle_Z^E(r) = \frac{3}{2}\cos^2\left[\frac{\pi}{2} - \phi(r)\right] - \frac{1}{2} = -\langle P_2\rangle_r(r) + \frac{1}{2}. \tag{8}$$

These quantities are plotted together with the simulation data for comparison of both procedures in Figs. 7 and 8. The elastic theory predictions are in good agreement with the simulation data for the smaller thicknesses (high values of r_1) for which the results of the two approaches are indeed very similar. Even though the profiles of the simulation data and of the theoretical curve have some similarities, for larger thicknesses, there are also some deviations between the results. This can be probably due to the fact that the LL potential is a nearest neighbor one and the boundary conditions effects propagate up to 1-2 lattice spacing. Then, for the larger thicknesses, at the middle of the cylindrical film, the aligning effect of the potential overcomes the surface effects.

V. POLARIZED MICROSCOPY OPTICAL IMAGES

To qualitatively appreciate the differences between the two cases studied here, we have also simulated the polarizing microscopy textures which have proved useful to investigate other confined nematic systems, such as droplets [13–15], planar

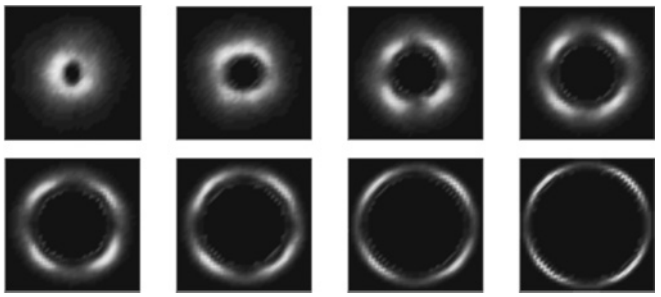

FIG. 10. Optical images (top view) as obtained by Monte Carlo simulations for the Z-R-BC case and different radii of the inner cylinder, i.e., $r_1 = 2,4,6,8,10,12,14,16$ (from top left to bottom right).

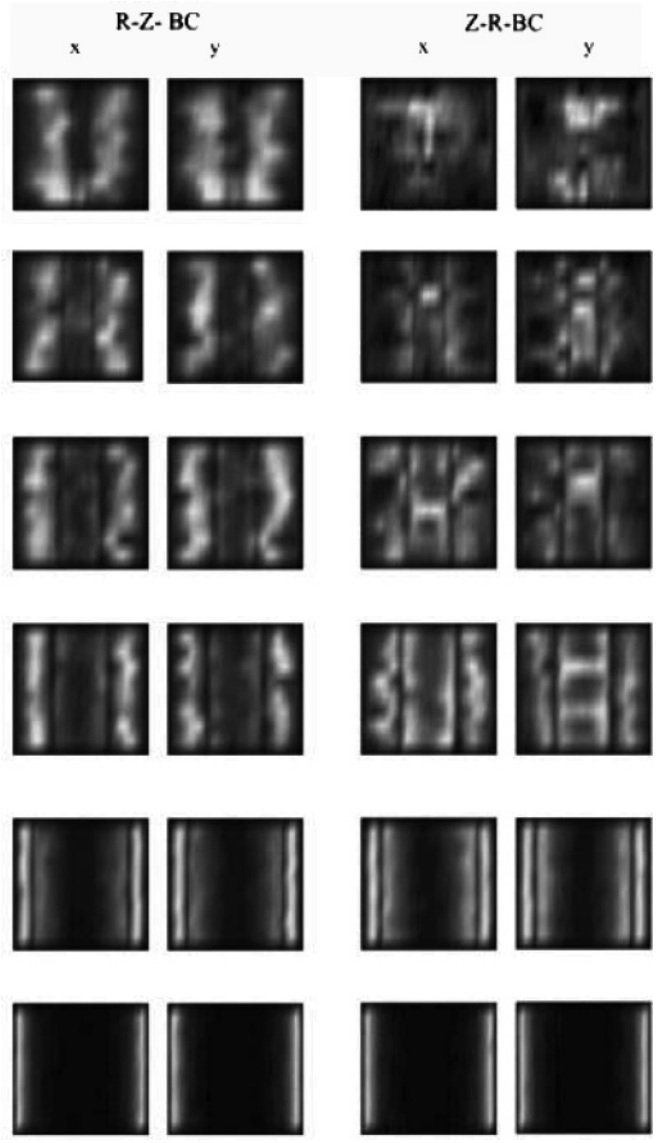

FIG. 11. Lateral views of the optical images as obtained by Monte Carlo simulations for the two boundary cases and different radii of the inner cylinder, i.e., $r_1 = 2,4,6,8,14,18$ (from the top to the bottom).

films, and twisted nematic display cells [16–18]. The textures were simulated by means of a Muller matrix approach [27], assuming, as usual, that the molecular domains represented by the spins act as optical retarders on the light propagating through the sample [28]. The following parameters were employed for computing the optical textures: film thickness $d = 5.3\ \mu$m, ordinary and extraordinary refractive indices $n_o = 1.5$ and $n_e = 1.66$, respectively, and light wavelength $\lambda_0 = 545$ nm [29,30]. The results are presented in Figs. 9 (top views), 10 (top views), and 11 (lateral views). Also from these images it is clear that no appreciable differences can be seen between the two boundary cases for the smaller thicknesses, while the optical patterns are different and distinguishable for the thicker film.

VI. CONCLUSIONS

We have studied a nematic confined between concentric cylindrical surfaces with different alignments. We have tackled the problem by means of Monte Carlo simulations of a simple lattice spin model and elastic theory. The simulation results of the ordering inside the cylindrical film are in a fair agreement with the analytical predictions for the various film thicknesses. The agreement between the simulations and the theory improves as the thickness decreases. In the theory we have neglected any possible spatial dependence of the elastic constant. This approximation works well when the separation between the cylinders is small. In addition, we remark that the order parameter obtained from the simulation varies with the position inside the film, while the one intervening in the spatial dependence of the elastic constant is essentially unchangeable [25]. We have also switched the surface alignments (firstly radial at the outer surface and aligned along Z at the inner surface, and secondly the opposite boundary ordering), and the results are indistinguishable for the cases when the film is sufficiently thin. These results are also confirmed by the elastic theory. To have a qualitative view, which can be eventually observed in real experiments, we have simulated the optical images as obtained by polarizing microscopy.

ACKNOWLEDGMENTS

L.R.E. and R.T.S. are grateful to Brazilian agencies CAPES, CNPq, and INCT-FCx. C.C. and P.P. acknowledge support by INFN Grant No. I.S. BO62.

[1] *Liquid Crystals in Complex Geometries*, edited by G. P. Crawford and S. Zumer (Taylor & Francis, London, 1996), and references therein.
[2] *Advances in the Computer Simulations of Liquid Crystals*, edited by P. Pasini and C. Zannoni (Kluwer, Dordrecht, 2000).
[3] I. V. Kotov, M. V. Khazimullin, and A. P. Krekhova, Mol. Cryst. Liq. Cryst. **366**, 2737 (2001).
[4] H. Tsuru, J. Phys. Soc. Jpn. **59**, 1600 (1990).
[5] D. R. M. Williams and A. Halperin, Phys. Rev. E **48**, R2366 (1993).
[6] P. G. de Gennes and J. Prost, in *The Physics of Liquid Crystals*, 2nd ed. (Clarendon Press, Oxford, 1993), p. 158.
[7] D. R. M. Williams, Phys. Rev. E **50**, 1686 (1994).
[8] R. Teixeira de Souza, J. C. Dias, R. S. Mendes, and L. R. Evangelista, Physica A **389**, 945 (2010).
[9] C. A. R. Yednak, R. Teixeira de Souza, G. G. Lenzi, E. K. Lenzi, and L. R. Evangelista, Mol. Cryst. Liq. Cryst. **526**, 82 (2010).
[10] C. A. R. Yednak, E. K. Lenzi, and L. R. Evangelista, Braz. J. Phys. **39**, 312 (2009).
[11] A. Corella-Maduenño, A. Castellanos-Moreno, S. Gutiérrez-Loópez, R. A. Rosas, and J. A. Reyes, Phys. Rev. E **78**, 022701 (2008).
[12] G. Bevilacqua and G. Napoli, Phys. Rev. E **81**, 031707 (2010).

[13] C. Chiccoli, P. Pasini, F. Semeria, and C. Zannoni, Phys. Lett. A **150**, 311 (1990).
[14] E. Berggren, C. Zannoni, C. Chiccoli, P. Pasini, and F. Semeria, Chem. Phys. Lett. **197**, 224 (1992).
[15] E. Berggren, C. Zannoni, C. Chiccoli, P. Pasini, and F. Semeria, Phys. Rev. E **50**, 2929 (1994).
[16] C. Chiccoli, O. D. Lavrentovich, P. Pasini, and C. Zannoni, Phys. Rev. Lett. **79**, 4401 (1997).
[17] C. Chiccoli, P. Pasini, I. Feruli, and C. Zannoni, Mol. Cryst. Liq. Cryst. **398**, 195 (2003).
[18] C. Chiccoli, P. Pasini, A. Sarlah, C. Zannoni, and S. Zumer, Phys. Rev. E **67**, 050703 (2003).
[19] C. Chiccoli, P. Pasini, F. Semeria, E. Berggren, and C. Zannoni, Mol. Cryst. Liq. Cryst. **290**, 237 (1996).
[20] N. Priezjev and Robert A. Pelcovits, Phys. Rev. E **62**, 6734 (2000).
[21] See, for example, T. Jin, B. Zalar, A. Lebar, M. Vilfan, S. Zumer, and D. Finotello, Eur. Phys. J. E **16**, 159 (2005).
[22] P. A. Lebwohl and G. Lasher, Phys. Rev. A **6**, 426 (1972).
[23] U. Fabbri and C. Zannoni, Mol. Phys. **58**, 763 (1986).
[24] N. Metropolis, A. W. Rosenbluth, M. N. Rosenbluth, A. H. Teller, and E. Teller, J. Chem. Phys. **21**, 1087 (1953).
[25] G. Barbero and L. R. Evangelista, *An Elementary Course on the Continuum Theory for Nematic Liquid Crystals* (World Scientific, Singapore, 2001).
[26] I. W. Stewart, *The Static and Dynamical Continuum Theory of Liquid Crystals* (Taylor & Francis, London, 2004).
[27] A. Killian, Liq. Cryst. **14**, 1189 (1993).
[28] R. Ondris-Crawford, E. P. Boyko, B. G. Wagner, J. H. Erdmann, S. Zumer, and J. W. Doane, J. Appl. Phys. **69**, 6380 (1991).
[29] C. Chiccoli, I. Feruli, P. Pasini, and C. Zannoni, in *Defects in Liquid Crystals: Computer Simulations, Theory and Experiments*, edited by O. D. Lavrentovich, P. Pasini, C. Zannoni, and S. Žumer, Chap. 4 (Kluwer, Dordrecht, 2001).
[30] E. Berggren, C. Zannoni, C. Chiccoli, P. Pasini, and F. Semeria, Int. J. Mod. Phys. C **6**, 135 (1995).